



Sources, Mechanisms, and Timescales of Sediment Delivery to a New England Salt Marsh

H. E. Baranes¹ , J. D. Woodruff¹, W. R. Geyer² , B. C. Yellen¹ , J. B. Richardson¹ , and Frances Griswold¹ 

¹Department of Geosciences, University of Massachusetts Amherst, Amherst, MA, USA, ²Applied Ocean Physics & Engineering Department, Woods Hole Oceanographic Institute, Falmouth, MA, USA

Key Points:

- Marine sediment mobilized and delivered during coastal storms is a primary source to a typical New England mesotidal salt marsh
- Suspended sediment in the estuary is highly non-stationary, with timescales of marine sediment delivery ranging from 2.5 days to 2 weeks
- Findings provide insight into sediment sources for small mesotidal estuaries and the more routine compounding impacts of annual storms

Supporting Information:

Supporting Information may be found in the online version of this article.

Correspondence to:

H. E. Baranes,
hbaranes@gmri.org

Citation:

Baranes, H. E., Woodruff, J. D., Geyer, W. R., Yellen, B. C., Richardson, J. B., & Griswold, F. (2022). Sources, mechanisms, and timescales of sediment delivery to a New England salt marsh. *Journal of Geophysical Research: Earth Surface*, 127, e2021JF006478. <https://doi.org/10.1029/2021JF006478>

Received 12 OCT 2021

Accepted 6 FEB 2022

Author Contributions:

Conceptualization: J. D. Woodruff, W. R. Geyer, B. C. Yellen

Data curation: B. C. Yellen

Formal analysis: J. D. Woodruff, W. R. Geyer, B. C. Yellen, J. B. Richardson, Frances Griswold

Funding acquisition: J. D. Woodruff, B. C. Yellen

Investigation: J. D. Woodruff, W. R. Geyer, B. C. Yellen, Frances Griswold

Methodology: J. D. Woodruff, W. R. Geyer, B. C. Yellen, J. B. Richardson

Project Administration: J. D. Woodruff

© 2022. The Authors.

This is an open access article under the terms of the [Creative Commons Attribution License](https://creativecommons.org/licenses/by/4.0/), which permits use, distribution and reproduction in any medium, provided the original work is properly cited.

Abstract The availability and delivery of an external clastic sediment source is a key factor in determining salt marsh resilience to future sea level rise. However, information on sources, mechanisms, and timescales of sediment delivery are lacking, particularly for wave-protected mesotidal estuaries. Here we show that marine sediment mobilized and delivered during coastal storms is a primary source to the North and South Rivers, a mesotidal bar-built estuary in a small river system impacted by frequent, moderate-intensity storms that is typical to New England (United States). On the marsh platform, deposition rates, clastic content, and dilution of fluvially-sourced contaminated sediment by marine material all increase down-estuary toward the inlet, consistent with a predominantly marine-derived sediment source. Marsh clastic deposition rates are also highest in the storm season. We observe that periods of elevated turbidity in channels and over the marsh are concurrent with storm surge and high wave activity offshore, rather than with high river discharge. Flood tide turbidity also exceeds ebb tide turbidity during storm events. Timescales of storm-driven marine sediment delivery range from 2.5 days to 2 weeks, depending on location within the estuary; therefore the phasing of storm surge and waves with the spring-neap cycle determines how effectively post-event suspended sediment is delivered to the marsh platform. This study reveals that sediment supply and the associated resilience of New England mesotidal salt marshes involves the interplay of coastal and estuarine processes, underscoring the importance of looking both up- and downstream to identify key drivers of environmental change.

Plain Language Summary Salt marshes need an external supply of mineral sediment to survive. Understanding sources and physical mechanisms of sediment delivery is therefore critical to effective salt marsh management. Sediment can be sourced from land and delivered to marshes through rivers, or it can come from the ocean during high tides and storm surges; however, the relative importance of these sediment sources is uncertain for most marshes. Here, we show that ocean sediment mobilized and delivered during coastal storms is the primary source to the North/South River estuary, a typical New England salt marsh system. Within the marsh platform, mineral sediment is most abundant near the ocean, and we find little river-derived sediment beyond the most landward region of the estuary. In estuary channels, we also observe the greatest amounts of suspended sediment when incoming tides flood the estuary during coastal storms. In contrast, we do not observe elevated suspended sediment when river flow is high. Our work shows that coastal and marine processes influence sediment supply and the associated resilience of New England salt marshes, underscoring the importance of looking both up- and downstream to identify key drivers of environmental change.

1. Introduction

Tidal salt marshes are critical protectors of the coast; they buffer against erosion and flooding (Möller et al., 2014), sequester carbon (Chmura et al., 2003), provide habitat to juvenile species and migratory birds (Boesch & Turner, 1984; Hughes, 2004), and filter pollutants and excess nutrients (Sousa et al., 2010). Coastal wetland maintenance involves complex biophysical feedbacks between clastic (i.e., inorganic) sediment supply, nutrients, plant growth, and flooding (Deegan et al., 2012; Kirwan & Megonigal, 2013). Deposition of clastic sediment in the form of clays, silts, and sands allows marshes to accrete faster than would be possible via in-situ organic production alone; thus, the availability and delivery of clastic sediment is a key factor in determining salt marsh resilience to erosion and future sea level rise (e.g., Donatelli et al., 2018; Fagherazzi et al., 2012; Ganju, 2019; Ganju et al., 2017; Kirwan et al., 2010; Liu et al., 2021; Morris et al., 2016; Redfield, 1972).

Resources: J. D. Woodruff, W. R. Geyer, B. C. Yellen, Frances Griswold
Supervision: J. D. Woodruff
Validation: W. R. Geyer, B. C. Yellen
Writing – review & editing: J. D. Woodruff, W. R. Geyer, B. C. Yellen, J. B. Richardson, Frances Griswold

Clastic sediment can be supplied by external fluvial and marine sources, or it can be derived internally from erosion of tidal flats and the marsh platform. In microtidal embayments (tide range <2 m), where the marsh edge is exposed to open water, storm surge and waves are dominant agents of erosion of tidal flat and marsh edge sediment and subsequent delivery to the marsh platform (Cahoon, 2006; Fagherazzi & Priestas, 2010; Fagherazzi et al., 2013; Mariotti & Fagherazzi, 2013; Reed, 1989; Turner et al., 2006). In contrast, wave-protected mesotidal marshes (tide range 2–4 m), which account for ~25% of marshes globally, fringe dendritic creek networks rather than large embayments; thus tides, fluvial processes, and channel morphology are additional important controls on sediment distribution (e.g., Fitzgerald et al., 2020a; Hopkinson et al., 2018; Leonard, 1997; Reed et al., 1999; Ward, 2004). In these mesotidal estuaries, uncertainty around sources, mechanisms, pathways, and timescales of sediment delivery through estuary channels and onto the marsh platform is widely recognized as an impediment to assessing marsh resilience to future sea level rise (Fagherazzi et al., 2018).

Sediment sourcing and delivery mechanisms are especially uncertain in mesotidal marshes in the New England region of the northeastern United States marshes given the heterogeneity of the region's post-glacial coastline (e.g., FitzGerald & van Heteren, 1999; Woodruff et al., 2021) and the substantial history of human impacts, including damming, deforestation (e.g., Foster & Motzkin, 2003), and coastal construction (e.g., groins, jetties, bulkheads, and revetments). Here, we define the mesotidal New England coast as the northern shore of Cape Cod through Maine-Canada border. Small salt marsh/estuarine complexes with relatively low fluvial sediment yields are common to this region (e.g., Meade, 1969; Millman & Farnsworth, 2011; Ralston et al., 2021; Weston, 2014), and frequent, moderate-intensity extratropical cyclones are the primary cause of flooding (e.g., Baranes et al., 2020; Kirshen et al., 2008). The great diurnal tide range increases northward from ~3 m in Massachusetts to ~6 m at the Canadian border, exceeding even the most extreme storm surges for the region (~1.3 m; Talke et al., 2018).

The few existing studies of sediment sourcing to New England marshes have widely ranging conclusions. Kirwan et al. (2011) and Braswell et al. (2020) proposed that deforestation by European colonists provided an upland sediment source that drove Northeastern marsh expansion in the eighteenth and nineteenth centuries. At the Webhannet River Estuary in Maine, Ward (2004) also concluded that the uplands were a significant modern-day sediment source based on observations of higher suspended sediment concentrations in the upper estuary channel than in the lower estuary.

In contrast, at the Plum Island Sound estuary in northern Massachusetts, Hopkinson et al. (2018) found that the watershed only supplied 8% of the clastic sediment required for the marsh to build elevation at the rate of present-day sea level rise. Marsh edge erosion supplied an additional 31%. Thus, they inferred that sediment input from tidal flat resuspension and marine environments were likely the most significant sources. Most recently, Fitzgerald et al. (2020a, 2020b) found that sediment-laden ice rafted onto the marsh surface during the winter storm season was a significant source to Great Marsh in Barnstable, MA (for example, a January 2018 Nor'easter delivered the equivalent of 15 years of clastic sediment).

Here, we combine sub-hourly turbidity observations with measurements of seasonal and centennial-timescale marsh platform clastic deposition to the mesotidal North and South River estuaries in Marshfield and Scituate, Massachusetts. Primary study goals include assessing: (a) the relative significance of marine, fluvial, and internally derived sediment sources; (b) the mechanisms and timescales of sediment delivery to the estuary; and (c) the role of tides and storms in modulating sediment delivery to the tidal creek network and marsh platform. We hypothesize that marine sediment is the primary clastic sediment source to the North and South River estuaries. New England watersheds have relatively low sediment yields, while high erosion rates along the coastline adjacent to the North and South Rivers (Theiler et al., 2013; U.S. Air Force, 2014) likely provide an important yet understudied sediment source. Moreover, we hypothesize that coastal storms combined with high spring tides are the most significant mechanisms of sediment delivery to the system because they drive the greatest flow velocities and water depths in the channel and over the marsh platform.

2. Methods

2.1. Site Description

The North/South River system is ideal for investigating marsh sediment sourcing in New England (Figure 1). The paired estuaries are connected to Massachusetts Bay via a shared barrier beach inlet. The 1898 Portland Gale

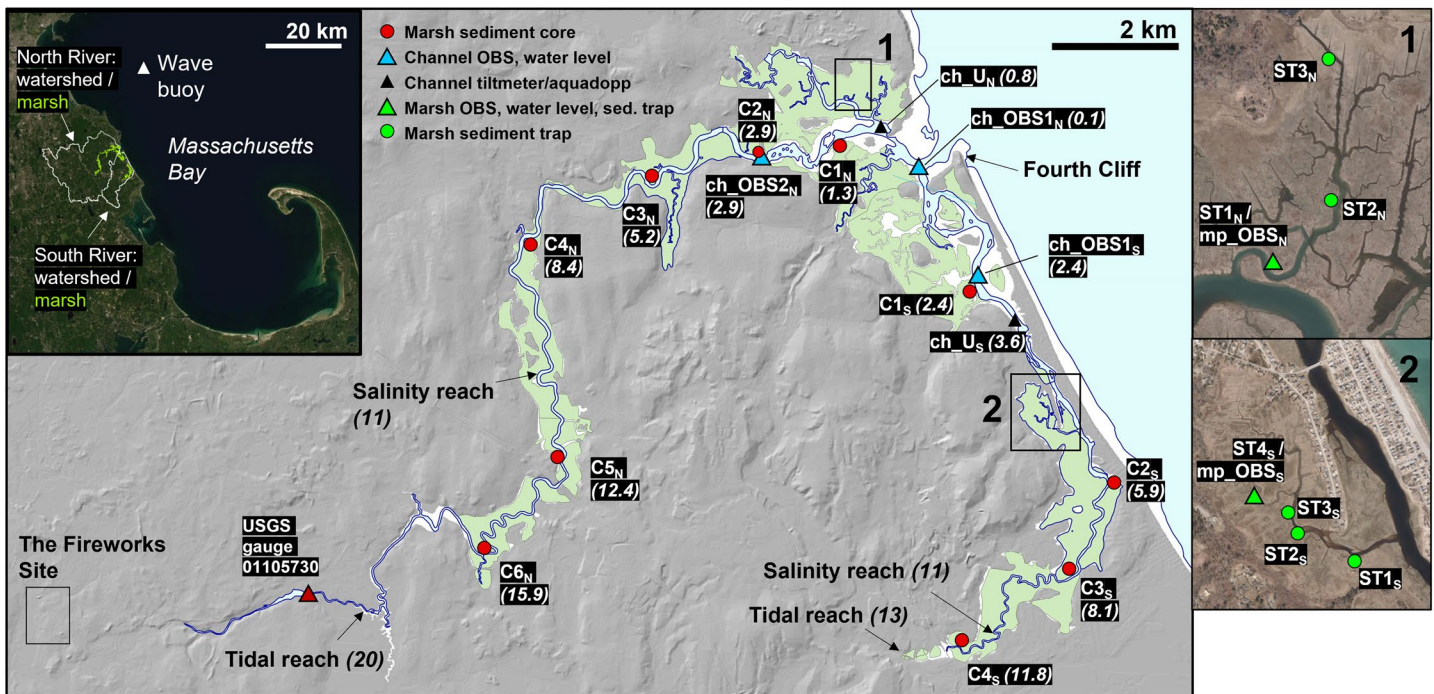


Figure 1. North and South River estuaries map, showing locations of field measurements. Italicized numbers in parentheses following location names indicate the distance up-estuary from the inlet in kilometers.


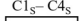
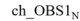

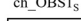
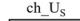


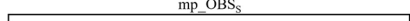
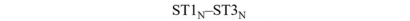
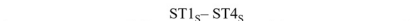
shifted the inlet 5.6 km to the north (to its present location) such that the North River estuary was shortened by over 25% (Johnson, 1925), and the elevation of mean high water (MHW) instantaneously increased 25 cm in the vicinity of the new inlet (Freitas & Ball, 1995; Yellen et al., 2022). In an accompanying paper, Yellen et al. (2022) find that marsh sediment deposition rates near the new inlet have been roughly double the rate of local relative sea level rise since 1898. Some abundant sediment source thus enabled the marsh to rapidly build elevation in response to a sudden increase in high water elevation.

The North River and South River channels are well-defined and constrained by high marsh platform for most of their courses. Channel widths are approximately 100 m within their seaward reaches and narrow up-estuary. Average thalweg depth is 5 m in the main channel. In the system's current configuration, the North River estuary has an 11-km salinity reach, a 20-km tidal reach (Figure 1), and contains 6.1 km² of tidal marsh (USFWS, 2013). The South River estuary is shallower and shorter, with thalweg depths of 2–4 m, an 11-km salinity reach, a 13-km tidal reach, and 5.2 km² of tidal marsh. The system has partially progressive, semidiurnal tides. Tide range at the inlet ranges 2–3.5 m (Kranenburg et al., 2019), and tidal attenuation results in the elevation of MHW decreasing by roughly 3.5 cm/km up-estuary (Yellen et al., 2022).

The coastline adjacent to the North and South River estuaries is eroding. Shoreline recession rates range from 0.1 to 0.5 m/year over the past century (Theiler et al., 2013), and approximately 1,150 m³ of sediment per year has been eroding from Fourch Cliff, the 0.5 km of coastline south of the North/South River inlet (Figure 1; U.S. Air Force, 2014). On the upland side, the relatively small 210 km² North River watershed is 38% urbanized (NLCD classes 21–24), with 20% water and wetland cover and 42% forest cover (USGS, 2016). The even smaller, 60 km² South River watershed is less urbanized (29%) with greater forest and wetland cover (64% and 22%, respectively).

In the estuary, low salt marsh areas are dominated by *Spartina alterniflora*, and high salt marsh is primarily *Spartina patens*. The tidal freshwater marsh is primarily *Typha angustifolia*. The marsh platform is also generally lower elevation in the North River than the South River. Marsh inundation depths are 30–80 cm at mean high water in the North River and 20–50 cm in the South River (Yellen et al., 2022). Sediment deposition rates vary throughout the estuary. In the South River salt marsh, 100-year average deposition rates are generally equivalent to the 100-year average sea level rise rate at the Boston NOAA tide gauge (2.9 mm/year). In the North River salt marsh, 100-year average deposition rates increase to between 5 and 10 mm/year (Yellen et al., 2022).

Table 1
Timetable of Channel and Marsh Platform Measurements From the North River (Black Bars) and South River (White Bars)

	2018		2020		
	Spring Mar 13–Apr 20	Fall Oct 4–Dec 6	Spring Mar 18–May 29	Spring May 29–Sep 9	Fall Sep 9–Dec 9
Marsh platform sediment cores	 				
Channel turbidity & water level	 				
Channel current					
Marsh platform turbidity & water level			 		
Marsh platform sediment traps			 		

Note. See Figure 1 for locations.

Both tropical and extratropical cyclones impact the region, and the most extreme storm surges reach 1.3 m (Talke et al., 2018). Extratropical cyclones have historically been the dominant flooding mechanism, as they are more frequent (25–30 tracks crossing northern New England per year; Fitzgerald et al., 2020a) and have longer durations more likely to intersect with high tides (e.g., Baranes et al., 2020; Kirshen et al., 2008; Talke et al., 2018). The 1898 Portland Gale, which drove one of the top-ten storm tides recorded in Boston since 1825 (2.8 m, with a 1.2-m skew surge; Talke et al., 2018) and moved the North/South River inlet 5.6 km to the north, likely represents the storm of record with respect to historical geomorphic alterations to the North/South River system (Fitzgerald, 1993).

2.2. Field Measurements

2.2.1. Field Measurements Overview

Field measurements from 2018 to 2020 include salt marsh sediment cores; seasonal sediment traps on the salt marsh platform; and water level, velocity, and turbidity measurements from both the channel and the marsh platform (Table 1, Figure 1). Locations with the subscript “N” are in the North River, and locations with the subscript “S” are in the South River. Distances for North and South Rivers are reported up-estuary from the confluence of the two estuaries at New Inlet (Figure 1).

2.2.2. Water Column Observations

We deployed channel instruments in the spring (March 13–April 20) and fall (October 4–December 6) of 2018. In the spring, pressure transducers for measuring water depth and optical-backscatter turbidity sensors (OBS) were deployed in the North River at 0.1 and 2.9 km (ch_OBS1_N and ch_OBS2_N, respectively; Figure 1). A Lowell Instruments tiltmeter for measuring water velocity at approximately 0.5 m above bottom was deployed in the South River at 3.6 km (ch_US; Figure 1). Measurements of atmospheric pressure were collected with an additional pressure transducer deployed in a nearby parking lot. Elevations of water level loggers deployed on rebar in shallow water were measured with a Real Time Kinematic (RTK) GPS. For deeper moored sites, sensor elevations were determined by measuring water surface elevation with a Post-Processing Kinematic GPS over the mooring for 1 min and then subtracting the average sensor-measured water depth during the same time interval.

Over the fall 2018 deployment period, we used the same pressure transducer and optical-backscatter turbidity mooring setup in the South River channel 2.4 km from the mouth (ch_OBS_S; Figure 1). We also deployed a bottom mounted Aquadopp acoustic Doppler current profiler (2 MHz) in the North River 0.8 km from the inlet (ch_UN). It provided velocity data at 20 cm increments from 0.6 m above bottom to 1 m below the water surface.

We used significant wave heights from the Boston wave buoy located ~20 km north of the estuary (NDBC buoy 44013) as a proxy for wave activity on the seaward side of the inlet and North River discharge at USGS gauge 01105730 (Figure 1) as proxy for freshwater input to the North and South Rivers. North River discharge is a reasonable proxy for temporal variation in South River discharge given their spatial proximity.

2.2.3. Marsh Platform Observations

In spring 2018, we collected sediment cores at six locations on the North River marsh between 1.3 and 15.9 km ($C1_N$ - $C6_N$; Figure 1) and four locations on the South River marsh between 2.4 and 11.8 km ($C1_S$ - $C4_S$; Figure 1). At each location, we collected a transect of cores perpendicular to the marsh edge using a 6.3-cm-diameter gouge corer. We observed minimal sediment compaction during collection (see also Yellen et al., 2022).

During the 2020 field seasons, we measured water level, turbidity, and seasonal sedimentation rates on areas of the marsh platform 1.7 km up-estuary from the inlet in the North River and 4.6 km from the inlet in the South Rivers (Figure 1). Sediment traps and sensors were placed within 5 m of the marsh edge such that they would capture a strong suspended sediment signal when the marsh was flooded from the channel. We mounted Onset HOBO U20L-04 pressure transducers and RBRsolo³ OBS sensors on rebar and sunk the rebar into marsh sediment such that the pressure transducer vents and OBS window were 4 cm above the marsh platform. We placed a 0.09 m² ceramic tile underneath the sensors to prevent grass from obstructing the OBS (see Figure S1 for a photo of the sensor setup). A field test of two RBR Solo³ OBS deployed in the same location with and without anti-fouling wipers showed that OBS on the marsh platform that go dry every low tide returned similar, high-quality measurements and thus generally did not require wipers. Pressure transducers recorded at a 10-min interval, and OBS recorded at a 5-min interval from March 18 through 9 December 2020. Records have 1-day lapses on May 29 and September 9 when we serviced and redeployed the instruments. As with the channel measurements, we deployed an additional subaerial pressure transducer to record atmospheric pressure, and we used an RTK GPS to measure the marsh platform elevation at all sediment traps and sensors.

Seasonal sediment traps consisted of 2.7-cm diameter 50 mL plastic centrifuge tubes with ¼-inch plastic mesh secured over their openings with rubber bands to keep out macrofauna such as crabs (Figure S1). Three to five replicate traps were sunk into the marsh surface ~10 cm apart such that the lip of each tube was 1 cm above the marsh surface. Results from early deployments showed that measurements were sufficiently reproducible to deploy three tubes per location. We collected and redeployed traps to measure spring (18 March 2020–29 May 2020), summer (29 May 2020–9 September 2020), and fall (9 September 2020–12 September 2020) sedimentation. We could not deploy traps or instruments in the winter due to water freezing in sediment traps and around sensors. Thus, winter sedimentation was not assessed, and our study excludes sediment delivered to the marsh via ice rafting (Argow et al., 2011; Fitzgerald et al., 2020b).

2.3. Sedimentary Analyses

We assessed sediment cores for downcore chemical variations via X-ray fluorescence (XRF) core scanning (Croudace et al., 2006) then selected one core from each location for further analyses. The selected cores were between 10 and 50 m from the marsh edge and representative of average marsh stratigraphy away from the edge. Proximity to the channel and bank slumping can drive anomalously high sedimentation rates (e.g., Coleman et al., 2020; Mariotti et al., 2016; Reed et al., 1999; Temmerman et al., 2003). We measured mass fractions of water, organic material, and inorganic sediment at 10 cm intervals in each core via loss on ignition (LOI; Dean, 1974). Sediment core age models were based on visual stratigraphic constraints and downcore profiles of short-lived radionuclides via gamma spectroscopy (see Yellen et al., 2022 for a detailed description).

We measured downcore lead (Pb) concentration in North River cores after XRF profiles revealed a traceable horizon of high Pb counts (Yellen et al., 2022). In brief, Pb concentrations were measured following USEPA Method 3050B using a hot-plate strong acid digestion. The digestate was diluted with 18.2 MΩ deionized water and analyzed with a Shimadzu 2030 Inductively Coupled Plasma-Mass Spectrometer. Every 25 samples included a duplicate, a standard reference material (NIST 2711b Montana Soil), and a digestion blank. Digestion blank Pb concentrations were <0.05 ng g⁻¹ measured concentrations, duplicates were within 12%, and NIST Montana Soil 2711b recoveries were between 87% and 96% of their certified values. We derived a relationship between XRF counts and Pb concentration via a linear regression of all measurements to estimate the full downcore profile of Pb concentrations from XRF counts (Figure S2; DiScenza et al., 2014).

Centrifuge tube sediment traps were capped in the field and brought to the laboratory for measuring clastic deposition rate over each seasonal deployment. We decanted and rinsed samples twice to remove salt, combusted them at 550°C, and weighed them to determine clastic mass via LOI. Clastic deposition rates were calculated as clastic mass divided by sediment trap cross-sectional area, divided by deployment time. To account for variability in the number of spring-neap tide cycles within each deployment, we normalized by the number of days the sediment trap site was inundated (determined via water level loggers deployed adjacent to the traps).

2.4. Moored Data Analyses

Measured pressure in the channel and on the marsh were converted to water depth (d , in m) by:

$$d = (P_w - P_A) / (\rho_w \times g)$$

where P_w is water pressure, P_A is atmospheric pressure, ρ_w is seawater density (assumed as 1,029 kg m⁻³), and g is gravitational acceleration (9.81 m s⁻²). Measurement errors in pressure were 0.1% of full scale, or about 2 cm depth, and vertical RTK measurement error was an additional 2 cm. For channel data, we then calculated the non-tidal residual using a 33-hr low-pass filter on the hourly water depths.

To clean channel OBS data, we first manually removed time intervals where turbidity rapidly fluctuated between low and anomalously high values. We then ran a wild-point editor 10 times that removed outliers greater than 4 standard deviations from a moving average. To clean marsh platform OBS data, we first used water levels from the same location to set turbidity to zero whenever the sensor was dry. We then manually removed time intervals when the sensor was clearly fouled or blocked, indicated by rapid fluctuations between high and low measurements or background turbidity gradually increasing without dropping back to zero when the sensor was dry at low tide. Turbidity often spiked to high values when the water surface crossed the sensor window on the flood or ebb tide, likely due to floating material at the water surface held by surface tension. We found that applying a 5-point median filter to the 5-min marsh platform turbidity data removed this effect.

3. Results

3.1. Channel Velocity and Turbidity

3.1.1. North River Channel

We compared the timing of distinct increases in channel turbidity to freshwater discharge and offshore wave height to identify the likely mechanistic driver of sediment delivery to the estuary and tidal marsh. In spring 2018, the time intervals with the highest observed turbidity in the North River at the ch_OBS2_N station (2.9 km from the inlet; Figure 1) were all concurrent with high offshore wave activity and a positive non-tidal residual, likely associated with storm surge (March 13–15, March 21–23, March 25–28, and April 15–17; Figures 2a and 2b). Overall, the onset and timescale of high-turbidity intervals in the North River channel were better aligned with 2 to 3-day coastal storms than with the longer period 2-week spring-neap cycle. River discharge was also elevated during storms over the spring 2018 deployment; however, the timing of high turbidity aligned closely with increases in offshore wave heights but not spikes in discharge. For example, the onset of high waves and high turbidity occurred on the same day during the March 21 storm and were followed by a more subtle increase in river discharge on March 22. Furthermore, there was no discernible turbidity response to high river discharge April 3–5, whereas all wave events over the deployment were concurrent with high turbidity.

Only the March 13 storm was recorded at the estuary inlet before the ch_OBS1_N sensor was buried on March 16. For three tide cycles during the storm, there was a strong pulse of turbidity on the flood tide that was greater in magnitude and arrived earlier at ch_OBS1_N relative to ch_OBS2_N 2.8 km up-estuary (Figure 2d). Over the subsequent three tide cycles, turbidity declined steeply at ch_OBS1_N and more gradually at ch_OBS2_N such that turbidity at ch_OBS2_N began to exceed that at ch_OBS1_N on March 15.

We also examined turbidity as a function of tide hour over various time intervals at the ch_OBS2_N station. For reference, Figure 3a shows velocity for a typical tide cycle at ch_OBS2_N; peak velocity was slightly higher on the flood tide (0.79 m s⁻¹) than on the ebb (−0.76 m s⁻¹), but high flow velocities were more prolonged on the ebb. Figure 3b shows ch_OBS2_N turbidity as a function of tide hour for individual tide cycles during time intervals

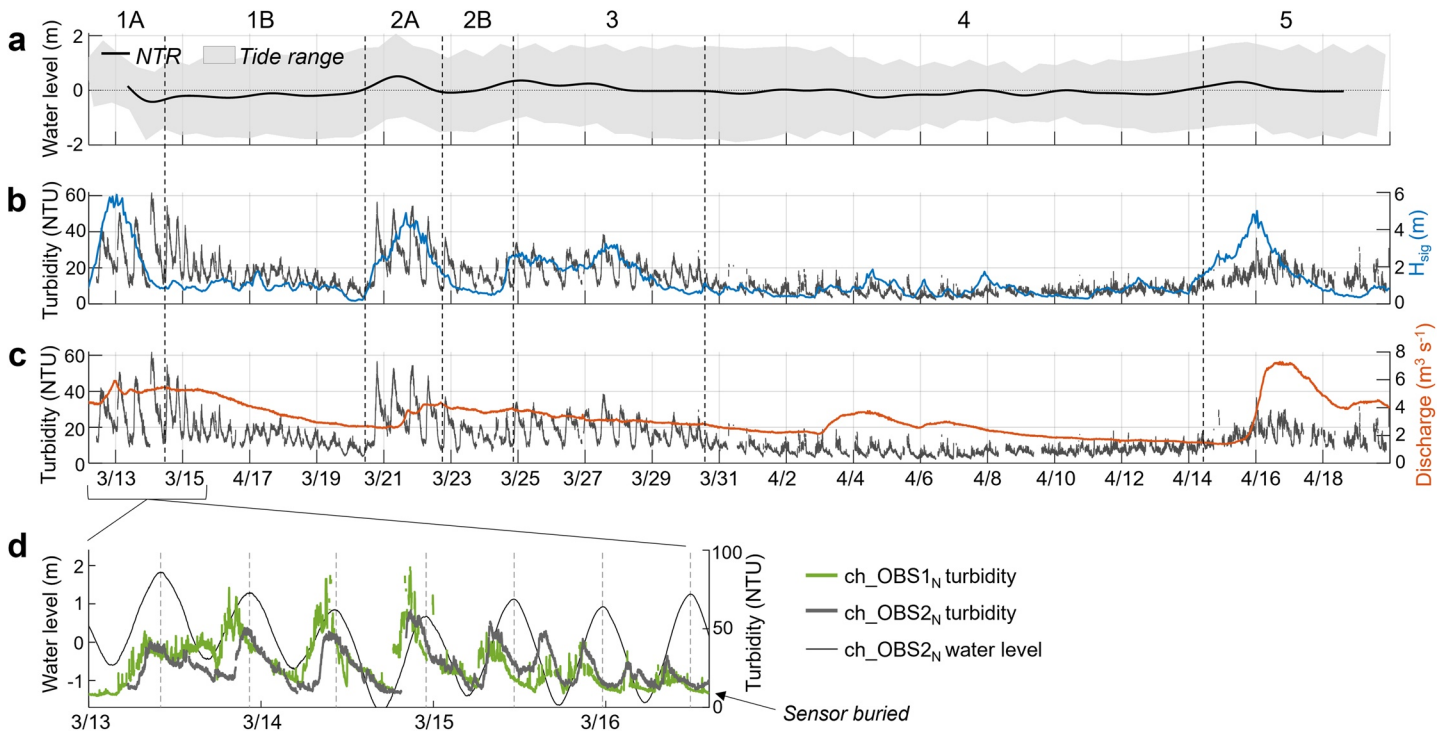


Figure 2. North River channel measurements for the spring 2018 deployment at ch_OBS2_N . Vertical dashed lines and labels above panel *a* mark time intervals in Figure 3. (a) Tide range (gray shading) and the non-tidal residual (black line) calculated from measured water levels. (b) Channel turbidity (gray line) relative to offshore significant wave height at the Boston wave buoy (blue line; see Figure 1 for buoy location). (c) Channel turbidity relative to North River discharge measured at the USGS gauge (red line; see Figure 1 for gauge location). (d) Close-up of the March 13 coastal storm, which was the only event recorded at the ch_OBS1_N inlet sensor before it was buried. ch_OBS1_N turbidity (green line) is shown alongside ch_OBS2_N turbidity (gray line) and water level (black line). Vertical dashed lines mark the timing of high tides.

labeled in Figure 2. Intervals 1 and 2A were concurrent with storm surge (i.e., a positive non-tidal residual) for the March 13 and 21 storms, while intervals 1B and 2B spanned the time from the end of surge until the beginning of the next storm. We could not calculate the non-tidal residual for the March 13 storm with a low-pass filter because it fell at the beginning of the deployment; thus, we assumed an equivalent 4-tide-cycle surge timescale for the March 13 and 21 storms. Flood tide turbidity significantly exceeded ebb tide turbidity during surge (intervals 1A & 2A) and became more balanced on the flood and ebb when surge ended (intervals 1B & 2B). Turbidity also remained high over the four tide cycles concurrent with storm surge and began to decline as soon as surge ended.

At the beginning of interval 3, two smaller coastal storms between March 25 and 27 also drove high flood-tide turbidity in the North River channel. Again, we observed turbidity declining when storm surge conditions ended on March 28. Interval 4 captured an extended period of lower wave activity, during which flood and ebb-tide turbidity measurements were roughly symmetric. Interval 5 was defined by a coastal storm with moderate wave heights and a rapid increase in river discharge to the highest values observed during the spring deployment. Turbidity during this period was elevated relative to the prior quiescent interval during both flood and ebb tides.

3.1.2. South River Channel

We also compared turbidity and water level observations collected from the South River channel during fall 2018 to offshore waves and river discharge (Figure 3). Turbidity and wave heights were generally low over the first 3 weeks of the fall deployment (October 5–27). An October 12 high discharge event that was equivalent to the peak discharge event observed during the spring deployment did not drive a discernible turbidity increase in the South River channel (Figure 3c). In contrast, a coastal storm on October 28 was concurrent with two tide cycles of anomalously high turbidity and marked a transition to stormier conditions (with wave events beginning October 28 and November 10, 16, and 25) and high turbidity in the South River channel that persisted through the remaining 5 weeks of the deployment. This prolonged high turbidity differs from spring North River observations, where turbidity dropped directly following surge and wave events (Figures 2 and 3b).

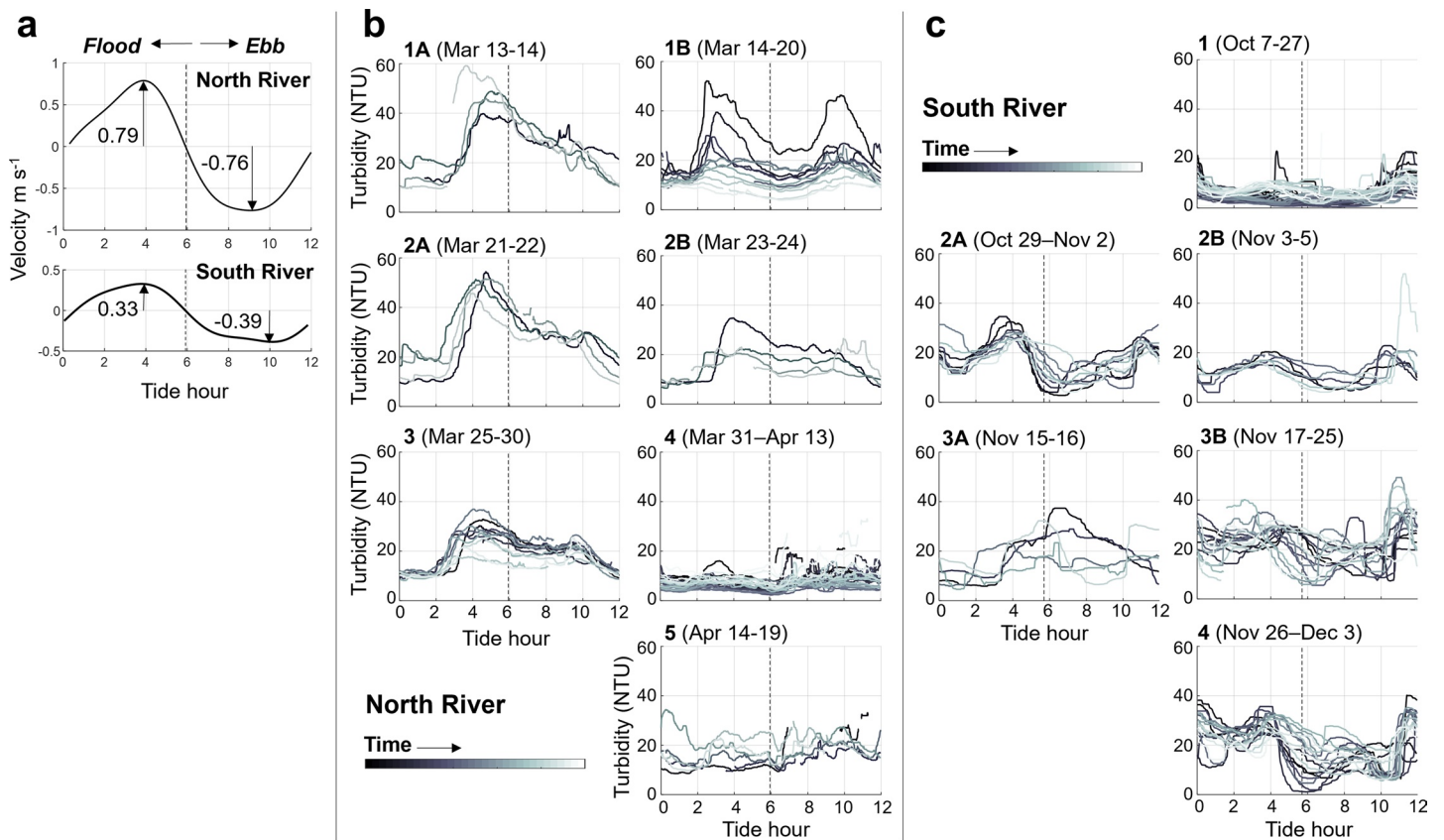


Figure 3. Turbidity and velocity versus tide hour at the ch_OBS2_N (North River) and ch_OBS_S (South River) sensors. (a) Velocity versus tide hour for a typical tide cycle at each sensor location, derived via harmonic analysis of water levels. Tide hour 0 is the beginning of flood tide at the inlet, and maximum and minimum velocities within the tide cycle are labeled. (b) North River ch_OBS2_N turbidity versus tide hour, where panels correspond to time intervals labeled in Figure 2. Each curve represents one tide cycle; the first tide cycle over each time interval is black, and lines get progressively lighter over subsequent tide cycles. The vertical dashed line in each panel delineates the flood and ebb tide. (c) South River ch_OBS_S turbidity versus tide hour, where panels correspond to time intervals labeled in Figure 4.

Figure 3 shows South River velocity and turbidity as a function of tide hour. At the moored locations, South River velocity was roughly half that observed in the North River (Figure 3a). Peak ebb velocity (-0.39 m s^{-1}) exceeded peak flood velocity (0.33 m s^{-1}), and high flow velocities were more prolonged on the ebb. There were extended periods within the South River deployment where turbidity measurements were noisy, likely due to organic material being trapped on the sensor window; thus, we limit our discussion of turbidity to intervals with high data quality. In the turbidity versus tide hour panels (Figure 3c), Interval 1 represents the period prior to the October 28 storm event when offshore wave heights and turbidity remained relatively low. Within each tide cycle over this initial quiescent interval, the highest turbidity was consistently at the end of the ebb tide. Intervals 2A-B represent observations following the October 28 storm (note that we exclude the two tide cycles concurrent with peak wave activity because turbidity values peaked above 300 NTU, likely due to obstruction of the sensor). Turbidity generally remained elevated and higher on the flood tide than the ebb tide for 5 days following the storm (Interval 2A, 10 tide cycles) before further decreasing and becoming more symmetric on the flood and ebb (Interval 2B). Intervals 3A-B and 4 show turbidity during and following the wave events that began November 16 and 25, respectively. For both events, storm surges (indicated by the positive non-tidal residual in Figure 4) did not align with large turbidity pulses (Intervals 3A, 4); however, a distinct turbidity peak persisted on the flood tide for 11 days following the November 16 storm (Interval 3B) and 10 days following the November 25 storm (Interval 4).

3.2. Marsh Platform Turbidity and Seasonal Deposition

We complement 2018 water column observations from the North and South River channels with similar observations from the marsh platform in 2020 (Figure 5). Water depths measured on the North and South River marsh

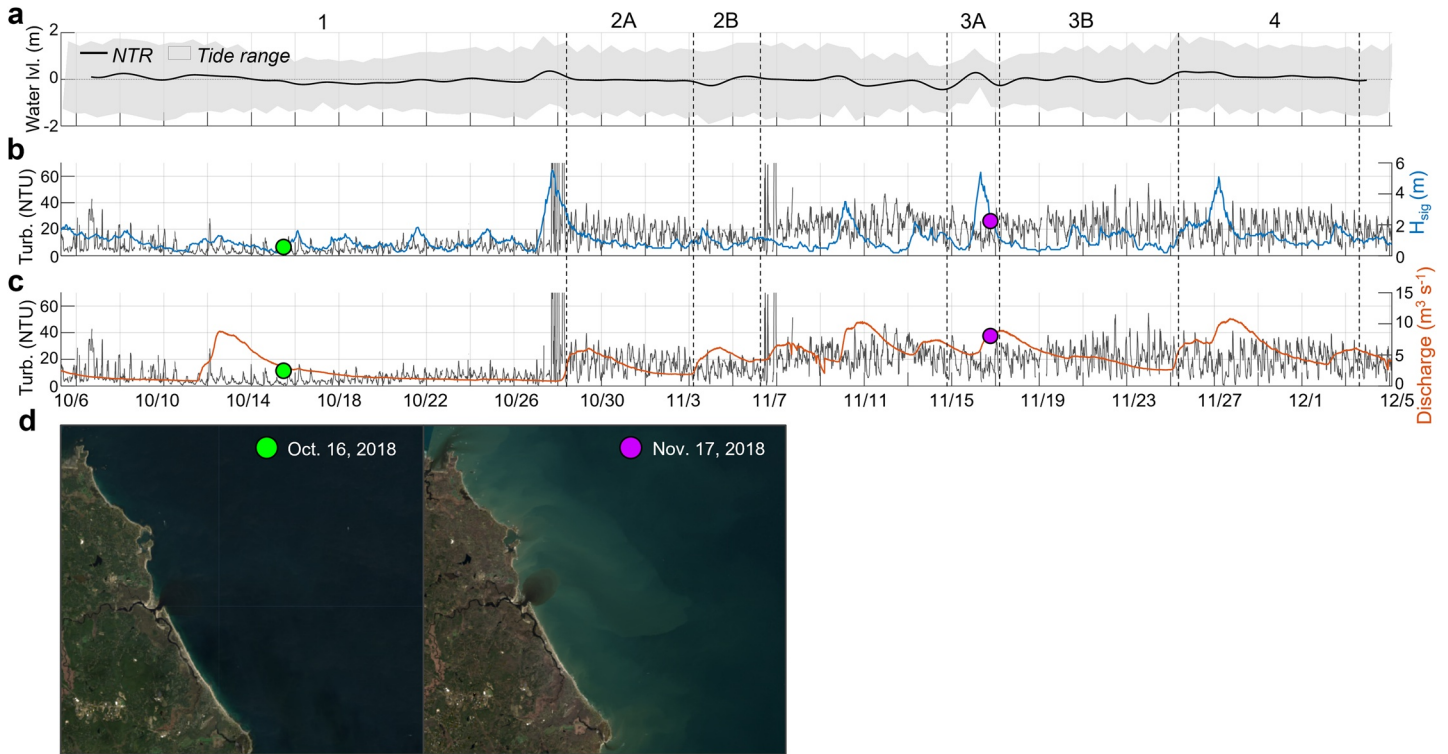


Figure 4. South River channel measurements for the fall 2018 deployment at ch_OBS_s. Vertical dashed lines and labels above panel *a* mark time intervals in Figure 3, and green and purple circles in panels *b*–*c* mark timing of satellite images in panel *d* (a) Tide range (gray shading) and the non-tidal residual (black line). (b) Channel turbidity (gray line) relative to offshore significant wave height at the Boston wave buoy (blue line). (c) Channel turbidity relative to North River discharge measured at the USGS gauge (red line). (d) Landsat 8 satellite images of the North and South River estuaries during non-storm (left) and storm (right) conditions.

show that the platform was inundated twice per day during spring tides and remained dry during neap tides (gray and light green filled regions in Figure 5b). Flood depths were generally within a few centimeters at the two sensors, but the South River site was inundated more frequently by low-amplitude high tides. At the location of the South River sensor, which was ~4 km farther up-estuary from the inlet than the North River sensor, tidal amplitude is smaller (due to tidal attenuation). Although marsh platform elevation is generally higher in the South River than the North River, the marsh is 15 cm lower at the location of the South River sensor (1.11 m NAVD88) than the North River sensor (1.26 m NAVD88).

The time intervals with the highest measured turbidity on the North River marsh platform aligned with concurrent wave and high discharge events on April 3 and 27 (Figures 5a and 5b; intervals 1 and 2). During both events, a strong pulse of high turbidity was observed over the North River marsh for 3–5 high tides (approximately the duration of storm surge), after which turbidity declined to background levels within 1 week (Figure 5c). Sediment delivery to the marsh over this 1-week post-event period differed for the April 3 and 27 storms: the April 3 storm occurred immediately before spring tides, so high spring tides continued driving high turbidity over the marsh directly following storm surge. Conversely, the April 27 event occurred during neap tides, so the marsh was only occasionally inundated over the subsequent 5 days, and turbidity had returned to lower background values by the following spring tides. The turbidity response during the April 3 and 27 events was more dispersed on the South River marsh than the North River marsh. Initial increases in over-marsh turbidity during these events were lower at the South River site, but the duration of elevated turbidity was longer, extending through the end of the following spring tides (Figure 5c). This corresponded to nine total days of elevated turbidity during and after the April 3 event and 14 days during and after the April 27 event.

Following these two storms, wave heights and river discharge were generally low mid-May through mid-August of 2020 (Figure 5a). During this quiescent summer interval, turbidity was usually higher over the South River marsh than the North River marsh, particularly over time periods when South River inundation depths were greater (e.g., late-May and mid-July).

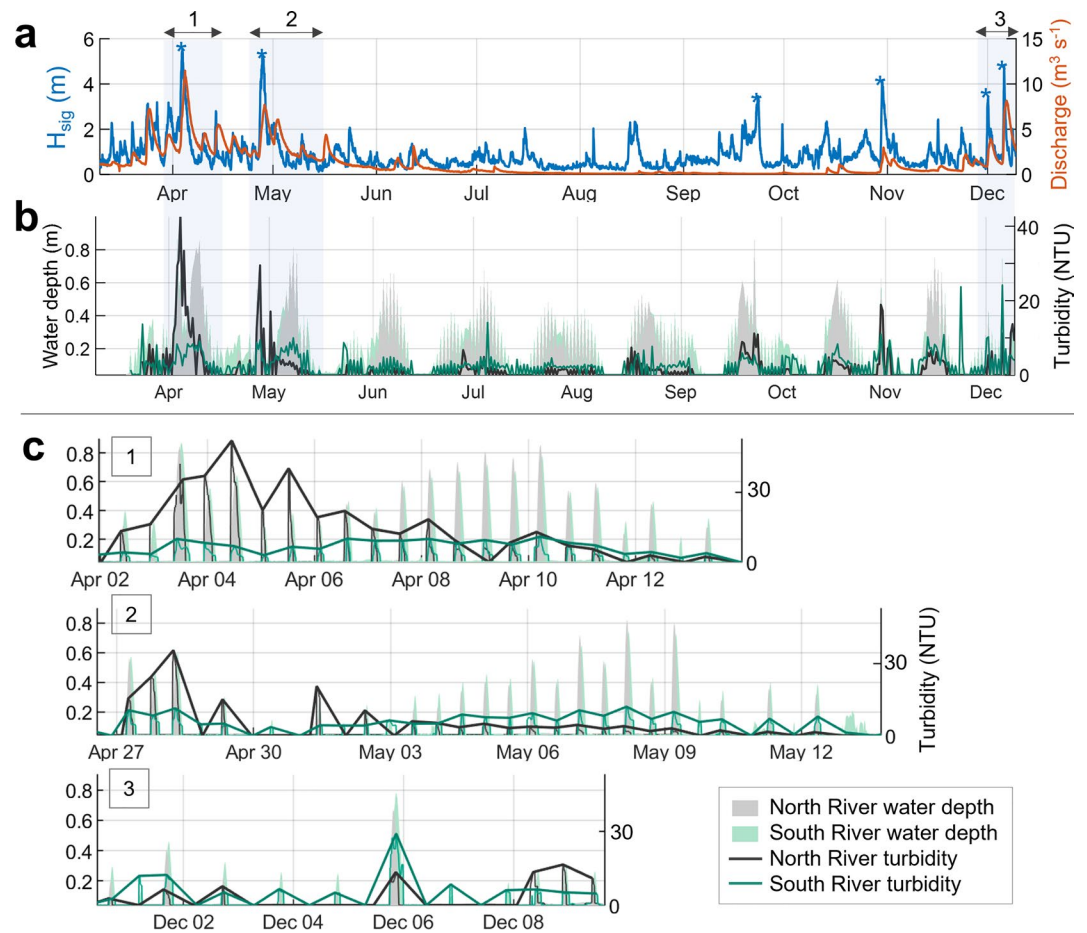


Figure 5. 2020 marsh platform moored observations at mp_OBS_N and mp_OBS_S. (a) Offshore wave heights at the Boston wave buoy (blue line) and North River discharge at the USGS gauge (red line). (b) Water depths over the North and South River marsh platforms (gray and green filled regions, respectively) and the maximum turbidity value measured over each tide cycle (black and green lines). Laboratory calibrations of these turbidity sensors show suspended sediment concentrations are roughly 1.8 times measured turbidity. (c) Enlarged time series for three offshore wave and high discharge events, with number labels corresponding to panels a–b. Note that the thin black and green lines show the full turbidity time series.

Two fall wave events on September 23 and October 30 again drove a greater turbidity response over the North River marsh than the South River marsh (Figures 5a and 5b). River discharge during the first of these wave events remained low, consistent with wave-induced mobilization and delivery of marine sediment to the estuary rather than fluvial sediment delivery (similar to findings from 2018 observations from the main channel). Both the September 23 and October 30 wave events occurred at the end of spring tides, and we observed no discernible turbidity response beyond the timescale of these events. In contrast to the previous four wave events discussed, offshore wave peaks on December 1 and 5 caused higher turbidity at the South River marsh sensor than the North River marsh sensor. Both these early-winter events were short in duration (1 tide cycle) and occurred during neap tides. Sensors were retrieved for the winter before capturing the post-event response during the spring tide following these December storms.

We complement the 2020 marsh time series data (Figure 5) with seven seasonal sediment traps deployed over the same time intervals (Table 2). Integrated seasonal accumulation of clastic material from these traps was consistent with higher sedimentation rates on the marsh platform in the spring and

Table 2
Seasonal Clastic Sedimentation Rates on the Marsh Platform Edge Measured by Sediment Traps

	Site	Clastic sedimentation rate (g/cm ² /y)		
		Spring	Summer	Fall
North River	ST1 _N	1.27	0.2	0.94
	ST2 _N	0.79	0.37	1.4
	ST3 _N	0.19	0.16	0.2
South River	ST1 _S	0.4	0.15	0.74
	ST2 _S	<i>not recovered</i>	0.25	0.48
	ST3 _S	0.26	0.11	0.24
	ST4 _S	0.25	0.11	0.85

Note. See Figure 1 for locations.

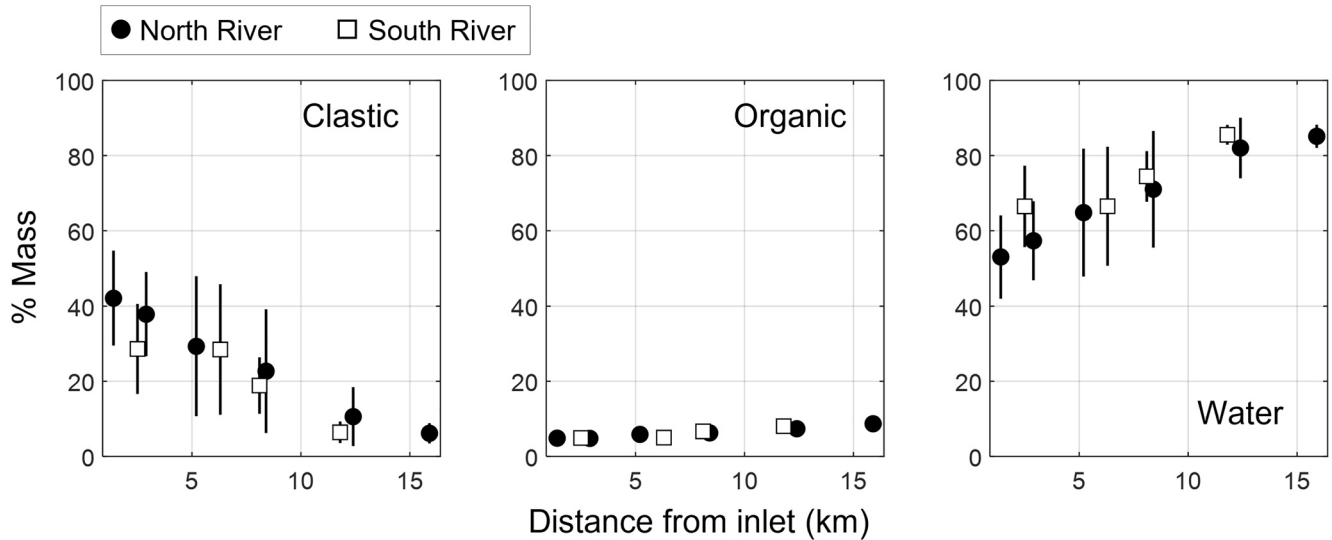


Figure 6. Variation in marsh platform sediment composition (in percent mass) with distance from the inlet in the North River (circles) and South River (squares). Point markers show mean mass percent of clastic sediment, organic material, and water, determined by loss-on-ignition of roughly 5 samples from the upper 50 cm of each core. Lines are one standard deviation of the mass percent data at each location.

fall relative to the quiescent summer season. Spatial variability in sedimentation rates among the trap locations was influenced by their relative distances from the marsh edge, marsh elevation, and along-channel distance from the sediment source (Temmerman et al., 2003).

3.3. Sediment Core Clastic Content and Pb Concentration

The clastic fraction of marsh platform sediment was highest near the inlet and decreased in the up-estuary direction (Figure 6). At C1_N (1.3 km from the inlet), the surficial 50 cm of the marsh was on average 42% clastic, 5% organic, and 53% water by mass. The clastic mass percent then gradually decreased up-estuary to 6% at C6_N, 15.9 km from the inlet. Clastic content was similar at equivalent distances from the inlet in the South River.

A horizon of high Pb concentration dating to the early 1900s (Yellen et al., 2022) was traceable in North River marsh at all core locations (Figure 7). Concentrations were highest in the upper estuary and decreased significantly in the mid and lower estuary. In the upper estuary landward of the salinity reach, the maximum measured Pb concentrations in the horizon were 4,160 parts per million (ppm) at C6_N (15.9 km from the inlet) and 3,740 ppm at C5_N (12.4 km). In the mid to lower estuary, concentrations monotonically decreased from 690 ppm at C4_N (8.4 km) to 310 ppm at C1_N (1.3 km). In the South River, we also found an early-1900s Pb horizon at C3_S, (8.1 km) and measured a maximum concentration of 260 ppm in the layer. The depth to the concurrent Pb horizon in each core illustrates along-estuary variation in marsh sedimentation rate. North River sedimentation rates near the inlet are roughly double those in the upper estuary, and the lowest sedimentation rates are in the South River (see also Yellen et al., 2022).

4. Discussion

4.1. Marine Sediment Sourcing

Marsh platform and channel observations both support our hypothesis that marine sediment is the primary clastic sediment source to the North and South River estuaries. In estuary channels, we directly observe coastal storms (indicated by periods of high waves and a positive non-tidal residual) rather than periods of elevated river discharge, driving the highest measured turbidity over the 2018 channel deployments. The highest-turbidity time intervals in the North River channel align with high offshore waves and storm surge (Figures 2a and 2b, Intervals 1a, 2a & 3) and are characterized by higher turbidity on the flood tide than the ebb tide (Figure 3). During the March 13–15 storm, before the ch_OBS1_N sensor was buried at the inlet (Figure 1), we also observe large flood-tide turbidity peaks at the inlet that appear 2 hrs later and are smaller in magnitude at ch_OBS2_N 2.8 km

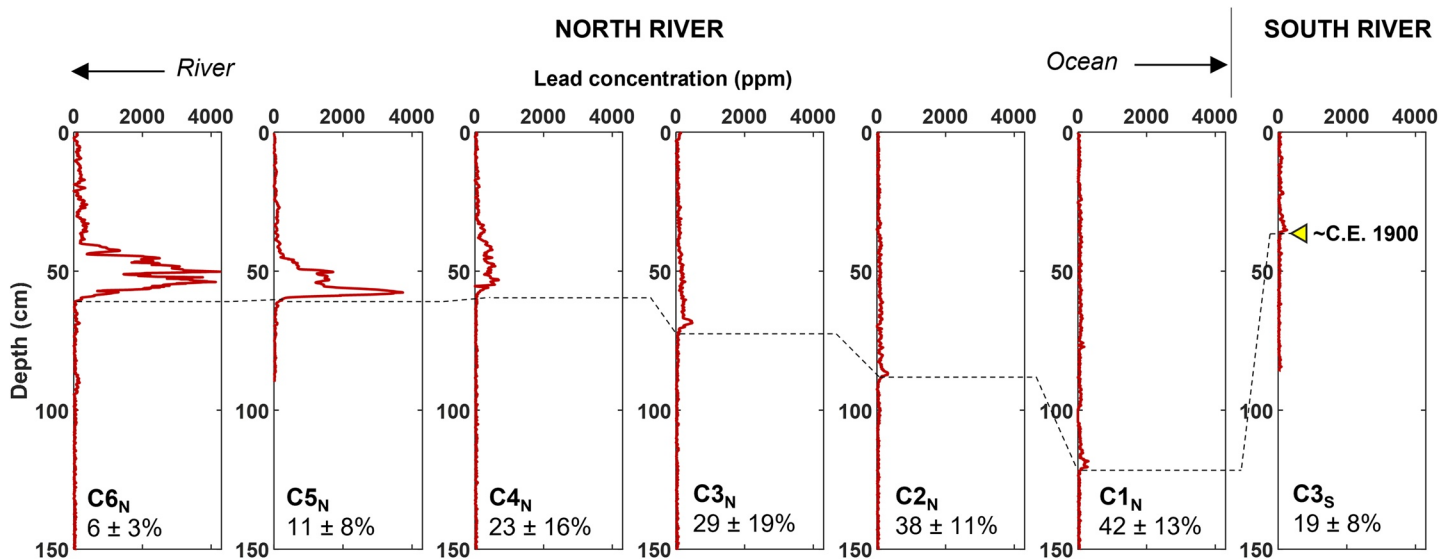


Figure 7. Pb concentration depth profiles from six representative North River cores (left six panels) and one South River core (rightmost panel) collected on the marsh platform. Concentrations are derived from an XRF counts-to-concentration calibration (Figure S2), and the dashed line marks the onset of and early-1900s contaminant horizon in each core (see Yellen et al., 2022 for age models). For reference, the mean and standard deviation percent clastic mass in the upper 50 cm of each core (relative to total wet mass) is listed below the core name in each panel.

up-estuary (Figure 2d). This delay and damping of turbidity are consistent with marine sediment entering through the inlet and being advected up-estuary on the flood tide. In the South River channel, turbidity does not fluctuate on the timescale of individual storm events, but a series of storms beginning on October 28 are concurrent with a prolonged 5-week period of high turbidity (Figure 4, intervals 2–4). Throughout the North and South River channel deployments, discharge is also often elevated during storms; however, high discharge intervals that do not align with coastal storms (e.g., April 3 and October 12) do not drive a significant turbidity response in the channels relative to the wave event response. Furthermore, the initial pulse of high turbidity during the March 21 (Figure 2c) and October 28 (Figure 4c) storms clearly precedes the rise in discharge.

We were unable to measure turbidity or suspended sediment concentration on the seaward side of the inlet during storms; however, a pair of cloud-free Landsat 8 satellite images of the North/South River estuary from October 16 and 17 November 2018, clearly show waves elevating offshore turbidity (Figure 4d). The October 16 image falls within the initial low-wave, low-turbidity, high-discharge period of our fall 2018 deployment. Ocean water is relatively clear, and the dark ebb plume, indicating higher concentrations of dissolved organic matter and lower concentrations of suspended sediment exiting the estuary through the inlet (e.g., Chen et al., 2020; Martinez et al., 2009), are consistent with our observation that discharge events do not deliver large sediment loads to the estuary. The November 17 image immediately follows high offshore waves and storm surge on November 15–16 and falls within a period of high turbidity in the South River channel (Figure 4). Coastal waters are filled with light-colored suspended sediment, and again, a dark ebb plume is visible exiting the estuary. These images further support coastal and near-shore erosion as the primary sediment source during storms, rather than upland sediment delivered via rivers or sediment derived internally from tidal flat and marsh edge erosion.

We had also hypothesized that storms and high spring tides would both be dominant mechanisms of sediment delivery to the North/South River estuary. We observe storms driving high turbidity in the channels, but we do not see evidence for two-week-timescale turbidity fluctuations that align with the spring-neap tidal cycle. This finding that storms deliver sediment to the North/South River estuary is significant because past observations (Fagherazzi & Priestas, 2010) and conceptual theory (Fagherazzi et al., 2013) have shown that storms driving strong tidal currents can also export significant amounts of sediment. We do not attempt the complex endeavor of quantifying sediment flux in tidal channels during storms (e.g., Ganju et al., 2013, 2017); however, multiple lines of evidence support storms primarily being a mechanism for sediment delivery to the North/South River estuary. First, time intervals with the highest measured channel turbidity align with coastal storms (Figures 2 and 4) and are characterized by higher turbidity on the flood tide than the ebb (Figures 3b and 3c). The November

17 satellite image is consistent with storms not exporting significant amounts of sediment in showing a dark ebb plume entering sediment-laden coastal waters immediately following the November 15–16 storm (Figure 4d). Lastly, clastic deposition rates on the marsh are higher in the stormy spring and fall seasons than the quiescent summer season (Table 2).

Marsh platform stratigraphy reinforces channel observations in supporting the hypothesis that marine sediment is a significant source to the North and South River estuaries. The early-1900s Pb contaminant horizon traces the limited spatial extent of fluvial sediment contributions. A former munitions manufacturing, testing, and disposal facility (called “The Fireworks Site”) located on a tributary to the North River in Hanover, MA is the most likely Pb source (Figure 1). The Fireworks Site began operations during World War I (1914–1918) and is known to have used Pb and mercury in its manufacturing processes (Town of Hanover, 2008) that has since been found in high concentrations in surrounding surface water, sediment, and fish tissue (Tetra Tech, 2005). We observe high Pb concentrations (~4,000 ppm) in the upper North River estuary freshwater tidal marsh platform above the salinity reach at C5_N and C6_N (Figure 7). In the mid-to-lower estuary, the combination of declining Pb concentration (Figure 7), increasing clastic content (Figure 6), and increasing sedimentation rates (Figure 7; Yellen et al., 2022) suggests significant dilution of contaminated fluvial sediment by a dominating marine clastic sediment source. In the South River marsh, we also observe an increase in clastic content toward the inlet that is consistent with marine sediment sourcing. Compared with the North River, the early-1900s Pb peak is more subtle in the South River, further supporting The Fireworks Site as the probable Pb source (Figure 7).

The relatively minor contribution of fluvial sediment in the North/South River estuary is consistent with findings at the Plum Island Sound estuary (~60 km to the north) that rivers only supply 8% of the clastic sediment required for the marsh to maintain its elevation relative to present sea level rise (Hopkinson et al., 2018). We do not measure fluvial suspended sediment concentrations, but sediment yields are relatively low throughout the New England region (e.g., Meade, 1969; Millman & Farnsworth, 2011; Ralston et al., 2021; Weston, 2014), and the North and South River watersheds have similar characteristics to the watersheds supplying Plum Island Sound in that they are low relief with relatively high freshwater wetland and forest land cover. By process of elimination, Hopkinson et al. (2018) infer that the combination of external marine and internal tidal flat sediment is the most significant sediment source to the Plum Island Sound estuary; however, they do not provide observational evidence for or delineate between the two sources due to the hydrodynamic complexity of the inlet (Zhao et al., 2010). In the smaller North-South River estuary, it is simpler to constrain transport and show that external marine sediment is the system's primary source, resulting in what we believe is the first observational study from the region to confirm marine sourcing.

Significant marine sediment delivery during storms is consistent with research findings in the North Sea. The salt marshes along the southern North Sea Coast in Denmark, Germany, and the Netherlands are globally the most comparable to New England marshes. Terrestrial sediment yields are low, and the coast is mesotidal and routinely impacted by winter storms of moderate intensity. Past periods of high accretion rates in Wadden Sea marshes have been connected to intervals of high storm activity (Schuerch et al., 2012); and similar to our observations in the North/South River Estuary, higher suspended sediment concentrations have been observed on the flood tide than the ebb during storm events (Bartholdy & Aagaard, 2001; Hache et al., 2021).

Elsewhere in the world, much of the research around marine storm impacts to marshes has focused on major river systems experiencing extreme human modifications and tropical cyclone-induced flood events. For example, in the Mississippi River and Changjiang Deltas, studies have found that the modern decline in riverine sediment inputs caused by dams and levees has been partially counteracted by marine sediment mobilized and delivered by waves and surge during tropical cyclones (Sanks et al., 2020; Smith et al., 2015; Wang et al., 2020). Our findings are therefore complementary to those along these major river systems in that we provide insight into another endmember: small estuaries impacted by more frequent and less intense extratropical storms.

4.2. Sediment Delivery Timescales and Marsh Platform Deposition

The spring-neap cycles is a dominant influence on sediment delivery from estuary channels to the marsh platform. Both in the channel and over the marsh, measured storm turbidity peaks are higher-magnitude and shorter in duration from sensors in the North River when compared to those deployed in the South River. In the North River channel, turbidity rapidly declines over 1–2 days after surge ends (e.g., Figure 3, intervals 1b & 2b). As a

result of this short duration of elevated sediment concentrations in the channel, the phasing of storm surge with the spring-neap cycle determines whether post-event suspended sediment is delivered to the marsh platform. For example, during spring tides we measure high turbidity at the North River marsh platform sensor for ~3 days following the April 3 storm (Figure 5b, interval 1). In contrast, the April 27 storm occurred during neap tides, and by the time spring tides returned to inundating the marsh platform on May 2nd, turbidity had dropped to background levels (Figure 5b, interval 2).

At the South River sensors, we observe high turbidity persisting for 5–11 days following storms in the channel (Figure 4, intervals 2a-b, 3a-b & 5) and 9–14 days on the marsh (Figure 5b), albeit at roughly half the turbidity values observed at our North River channel location. This longer period of elevated turbidity makes sediment delivery to the marsh platform less dependent on the phasing of events with the spring-neap cycle. In the case of the April 27 storm, high turbidity persists over the South River marsh platform for the entire spring tide following the storm (in contrast to the North River site), despite the storm occurring during neap tides.

Understanding the geomorphic drivers of the varying turbidity timescales between the North and South Rivers would require a greater spatial distribution of moored observations over longer, concurrent deployments. For example, cross-correlation analyses among spatial locations and as a function of the primary external forcings could improve the robustness of estimates of spatial variation in turbidity response time. However, we hypothesize that the lower elevation of the North River marsh relative to mean high water is a potential explanation. When the 1898 Portland Gale shifted the North/South River inlet 5.6 km to the north, North River mean high water elevation instantaneously increased because the truncated length of the estuary reduced tidal attenuation. Although North River sedimentation rates have been roughly double those observed in the South River since the inlet switch, the system is still adjusting (Yellen et al., 2022). It is well established that greater marsh platform inundation depths enhance deposition (e.g., Bricker-Urso et al., 1989; Marion et al., 2009; Pethick, 1981; Temmerman et al., 2003), so higher inundation depths on North River marsh platform may shorten the duration of high suspended sediment concentrations the channel due to enhanced trapping on the marsh. The relatively higher marsh elevations in the South River estuary lower the rate of sediment trapping. Storm-induced pulses of sediment should therefore be expected to remain in the South River channel for longer, explaining the longer storm response timescale of suspended sediment. The higher marsh platform also may explain the greater relative ebb turbidity in the South River under non-storm conditions. If less sediment is trapped on the marsh platform, more sediment must be exported to the ocean during non-storm conditions to approach a net sediment balance.

4.3. Implications of Coastal Armoring

Externally derived marine sediment supplying the North and South River estuaries implies that coastal and nearshore sediment supply and erosion rates influence marsh accumulation. In New England, surficial sediment sources in coastal and nearshore regions are primarily glacial-fluvial and glacial-lacustrine deposits (e.g., Woodruff et al., 2021). In the case of the North and South Rivers, adjacent shoreline recession (Theiler et al., 2013) and the rapid erosion of Fourth Cliff (Figure 1; U.S. Air Force, 2014) are potentially significant sediment sources.

Human decision-making impacts erosion at the coast and thus has the potential to impact marsh sediment supply. For example, in the Wadden Sea, Hache et al. (2020, 2021) observed that less than half the available suspended sediment mobilized during storms was able to accumulate on marshes behind artificial revetments and breakwaters. As of 2013, nearly 27% of the Massachusetts coastline was armored by some form of coastal protection (Fontenault et al., 2013). At Jamaica Bay Marsh in New York City, Peteet et al. (2018) suggested that hardening of the coast may have decreased clastic sediment delivery to the marsh, but they do not provide direct evidence for a link between armoring and sediment supply. To our knowledge, no further studies have attempted to assess the impacts of coastal armoring on suspended sediment availability in the Northeastern United States. Our finding that the North/South River estuary relies on an external marine sediment supply therefore underscores the need for further research on coastal armoring impacts.

5. Conclusions

This study provides clear evidence that marine sediment is the major clastic sediment source to marshes in a small, mesotidal estuarine system characteristic of the New England coastline. Spatial variation in marsh sediment clastic content and fluvially-sourced Pb pollution show that marine-sourced clastic sediment has been the

primary external sediment source in the mid-to-lower North and South River estuaries. We also observe sediment advected through the inlet during coastal storms as the primary driver of high turbidity in estuary channels and over the marsh platform. Thus, our observations are among the first to show external marine sediment mobilized during storms as the primary sediment source to the estuary, rather than terrestrial sediment delivered via rivers or internally derived sediment resuspended from tidal flats or eroded from the marsh edge.

Suspended sediment in the estuary is a highly non-stationary quantity, with timescales of sediment delivery ranging from 2.5 days to 2 weeks depending on the location within the estuary. In locations with shorter sediment residence times, the extent of sediment delivery from the channel to the marsh platform is dependent on timing of storms relative to the spring-neap tide cycle. This study reveals that sediment supply to New England mesotidal salt marshes and their associated resilience involves the interplay of coastal and estuarine processes. It is therefore important to look both up- and downstream to identify key drivers of environmental change. Globally, research around storm impacts to marshes has primarily focused on major river systems experiencing extreme human and tropical cyclone impacts. Our findings, along with similar past research in the North Sea, thus provide insight into another salt marsh endmember: small estuaries impacted by more frequent and less intense extratropical storms.

Conflict of Interest

The authors declare no conflicts of interest relevant to this study.

Data Availability Statement

All original data presented in this publication are available at <https://doi.org/10.7275/szte-xm56> under a Creative Commons Attribution 4.0 License. Wave buoy data are available at <https://www.ndbc.noaa.gov>, and river flow data are available at <https://waterdata.usgs.gov>.

Acknowledgments

The project described in this publication was in part supported by Grant or Cooperative Agreement No. G20AC00071 from the U.S. Geological Survey and a Department of Interior Northeast Climate Adaptation Science Center graduate fellowship awarded to H.E.B (G12AC00001). Its contents are solely the responsibility of the authors and do not necessarily represent views of the Northeast Climate Adaptation Science Center or the USGS. J. D. W. did initial analyses for this publication while in residency at the Darling Marine Center. The authors would also like to thank Tim Cook, Dave Ralston, Noa Randall, Stella Wenzel, Julia Casey, and Waverly Lau for their assistance with field work, lab work, and preliminary data analysis.

References

- Argow, B. A., Hughes, Z. J., & FitzGerald, D. M. (2011). Ice raft formation, sediment load, and theoretical potential for ice-rafted sediment influx on northern coastal wetlands. *Continental Shelf Research*, 31(12), 1294–1305. <https://doi.org/10.1016/j.csr.2011.05.004>
- Baranes, H. E., Woodruff, J. D., Talke, S. A., Kopp, R. E., Ray, R. D., & DeConto, R. M. (2020). Tidally driven interannual variation in extreme sea level frequencies in the Gulf of Maine. *Journal of Geophysical Research: Oceans*, 125(10), e2020JC016291. <https://doi.org/10.1029/2020JC016291>
- Bartholdy, J., & Aagaard, T. (2001). Storm surge effects on a back-barrier tidal flat of the Danish Wadden Sea. *Geo-Marine Letters*, 20, 133–141. <https://doi.org/10.1007/s003670000048>
- Boesch, D. F., & Turner, R. E. (1984). Dependence of fishery species on salt marshes: The role of food and refuge. *Estuaries*, 7(4), 460–468. <https://doi.org/10.2307/1351627>
- Braswell, A. E., Heffernan, J. B., & Kirwan, M. L. (2020). How old are marshes on the East Coast, USA? Complex patterns in wetland age within and among regions. *Geophysical Research Letters*, 47(19), e2020GL089415. <https://doi.org/10.1029/2020GL089415>
- Bricker-Urso, S., Nixon, S. W., Cochran, J. K., Hirschberg, D. J., & Hunt, C. (1989). Accretion rates and sediment accumulation in Rhode Island salt marshes. *Estuaries*, 12(4), 300–317. <https://doi.org/10.2307/1351908>
- Cahoon, D. R. (2006). A review of major storm impacts on coastal wetland elevations. *Estuaries and Coasts*, 29(6), 889–898. <https://doi.org/10.1007/BF02798648>
- Chen, J., Zhu, W., Tian, Y. Q., & Yu, Q. (2020). Monitoring dissolved organic carbon by combining Landsat-8 and Sentinel-2 satellites: Case study in Saginaw River estuary, Lake Huron. *The Science of the Total Environment*, 718, 137374. <https://doi.org/10.1016/j.scitotenv.2020.137374>
- Chmura, G. L., Anisfeld, S. C., Cahoon, D. R., & Lynch, J. C. (2003). Global carbon sequestration in tidal, saline wetland soils. *Global Biogeochemical Cycles*, 17(4). <https://doi.org/10.1029/2002GB001917>
- Coleman, D. J., Ganju, N. K., & Kirwan, M. L. (2020). Sediment delivery to a tidal marsh platform is minimized by source decoupling and flux convergence. *Journal of Geophysical Research: Earth Surface*, 125(8), e2020JF005558. <https://doi.org/10.1029/2020JF005558>
- Croudace, I. W., Rindby, A., & Rothwell, R. G. (2006). ITRAX: Description and evaluation of a new multi-function X-ray core scanner. *Geological Society, London, Special Publications*, 267(1), 51–63. <https://doi.org/10.1144/GSL.SP.2006.267.01.04>
- Dean, W. E. (1974). Determination of carbonate and organic matter in calcareous sediments and sedimentary rocks by loss on ignition; comparison with other methods. *Journal of Sedimentary Research*, 44(1), 242–248. <https://doi.org/10.1306/74D729D2-2B21-11D7-8648000102C1865D>
- Deegan, L. A., Johnson, D. S., Warren, R. S., Peterson, B. J., Fleeger, J. W., Fagherazzi, S., & Wollheim, W. M. (2012). Coastal eutrophication as a driver of salt marsh loss. *Nature*, 490(7420), 388–392. <https://doi.org/10.1038/nature11533>
- Disenza, D., Keimowitz, A., & Fitzgerald, N. (2014). Calibration and evaluation of an X-ray fluorescence method for the determination of lead and arsenic in soils. *International Journal of Environmental Analytical Chemistry*, 1, 103. <https://doi.org/10.4172/2380-2391.1000103>
- Donatelli, C., Ganju, N. K., Zhang, X., Fagherazzi, S., & Leonardi, N. (2018). Salt marsh loss affects tides and the sediment budget in shallow bays. *Journal of Geophysical Research: Earth Surface*, 123(10), 2647–2662. <https://doi.org/10.1029/2018JF004617>
- Fagherazzi, S., Kearney, W. S., Jiménez-Robles, A. M., Hopkinson, C., Castagno, K. A., & Ganju, N. K. (2018). *Assessing salt marsh resilience with sediment fluxes: The critical role of marine sediment inputs*, 2018.
- Fagherazzi, S., Kirwan, M. L., Mudd, S. M., Gunterpergen, G. R., Temmerman, S., D'Alpaos, A., et al. (2012). Numerical models of salt marsh evolution: Ecological, geomorphic, and climatic factors. *Reviews of Geophysics*, 50(1). <https://doi.org/10.1029/2011RG000359>

- Fagherazzi, S., & Priestas, A. M. (2010). Sediments and water fluxes in a muddy coastline: Interplay between waves and tidal channel hydrodynamics. *Earth Surface Processes and Landforms*, 35(3), 284–293. <https://doi.org/10.1002/esp.1909>
- Fagherazzi, S., Wiberg, P. L., Temmerman, S., Struyf, E., Zhao, Y., & Raymond, P. A. (2013). Fluxes of water, sediments, and biogeochemical compounds in salt marshes. *Ecological Processes*, 2(1), 3. <https://doi.org/10.1186/2192-1709-2-3>
- FitzGerald, D., Ryerson, O., Hughes, Z., Black, S., Georgiou, I., Hein, C., & Novak, A. (2020). Long-term variability in inorganic sediment contributions to the Great Marsh, Massachusetts. *Journal of Coastal Research*, 95(SI), 490–494. <https://doi.org/10.2112/SI95-095.1>
- FitzGerald, D. M. (1993). Origin and stability of tidal inlets in Massachusetts. In *Formation and evolution of multiple tidal inlets* (pp. 1–61). American Geophysical Union (AGU). <https://doi.org/10.1029/CE044p0001>
- FitzGerald, D. M., & Heteren, S. V. (1999). Classification of paraglacial barrier systems: Coastal New England, USA. *Sedimentology*, 46(6), 1083–1108. <https://doi.org/10.1046/j.1365-3091.1999.00266.x>
- FitzGerald, D. M., Hughes, Z. J., Georgiou, I. Y., Black, S., & Novak, A. (2020). Enhanced, climate-driven sedimentation on salt marshes. *Geophysical Research Letters*, 47(10), e2019GL086737. <https://doi.org/10.1029/2019GL086737>
- Fontenault, J., Vinhateiro, N., & Knee, K. (2013). *Mapping and analysis of privately-owned coastal structures along the Massachusetts shoreline* (p. 76). RPS ASA. Retrieved from <https://www.mass.gov/files/documents/2016/08/nk/private-coastal-structures-2013.pdf>
- Foster, D. R., & Motzkin, G. (2003). Interpreting and conserving the openland habitats of coastal New England: Insights from landscape history. *Forest Ecology and Management*, 185(1), 127–150. [https://doi.org/10.1016/S0378-1127\(03\)00251-2](https://doi.org/10.1016/S0378-1127(03)00251-2)
- Freitas, F., & Ball, D. (1995). *Warnings ignored! The story of the Portland Gale of 1898*.
- Ganju, N. K. (2019). Marshes are the new beaches: Integrating sediment transport into restoration planning. *Estuaries and Coasts*, 42(4), 917–926. <https://doi.org/10.1007/s12237-019-00531-3>
- Ganju, N. K., Defne, Z., Kirwan, M. L., Fagherazzi, S., D'Alpaos, A., & Carniello, L. (2017). Spatially integrative metrics reveal hidden vulnerability of microtidal salt marshes. *Nature Communications*, 8(1), 14156. <https://doi.org/10.1038/ncomms14156>
- Ganju, N. K., Nidziko, N. J., & Kirwan, M. L. (2013). Inferring tidal wetland stability from channel sediment fluxes: Observations and a conceptual model. *Journal of Geophysical Research: Earth Surface*, 118(4), 2045–2058. <https://doi.org/10.1002/jgrf.20143>
- Hache, I., Karius, V., & von Eynatten, H. (2020). Suspended particulate matter for sediment accumulation on inundated anthropogenic marshland in the southern North Sea—potential, thresholds and limitations. *Continental Shelf Research*, 207, 104214. <https://doi.org/10.1016/j.csr.2020.104214>
- Hache, I., Karius, V., & von Eynatten, H. (2021). Storm surge induced sediment accumulation on marsh islands in the southeastern North Sea: Implications for coastal protection. *Estuarine, Coastal and Shelf Science*, 263, 107629. <https://doi.org/10.1016/j.ecss.2021.107629>
- Hopkinson, C. S., Morris, J. T., Fagherazzi, S., Wollheim, W. M., & Raymond, P. A. (2018). Lateral marsh edge erosion as a source of sediments for vertical marsh accretion. *Journal of Geophysical Research: Biogeosciences*, 123(8), 2444–2465. <https://doi.org/10.1029/2017JG004358>
- Hughes, R. G. (2004). Climate change and loss of saltmarshes: Consequences for birds. *Ibis*, 146(s1), 21–28. <https://doi.org/10.1111/j.1474-919X.2004.00324.x>
- Johnson, D. W. (1925). *The New England-Acadian shoreline*. John Wiley & Sons.
- Kirshen, P., Knee, K., & Ruth, M. (2008). Climate change and coastal flooding in Metro Boston: Impacts and adaptation strategies. *Climatic Change*, 90(4), 453–473. <https://doi.org/10.1007/s10584-008-9398-9>
- Kirwan, M. L., Guntenspergen, G. R., D'Alpaos, A., Morris, J. T., Mudd, S. M., & Temmerman, S. (2010). Limits on the adaptability of coastal marshes to rising sea level. *Geophysical Research Letters*, 37(23). <https://doi.org/10.1029/2010GL045489>
- Kirwan, M. L., & Megonigal, J. P. (2013). Tidal wetland stability in the face of human impacts and sea-level rise. *Nature*, 504(7478), 53–60. <https://doi.org/10.1038/nature12856>
- Kirwan, M. L., Murray, A. B., Donnelly, J. P., & Corbett, D. R. (2011). Rapid wetland expansion during European settlement and its implication for marsh survival under modern sediment delivery rates. *Geology*, 39(5), 507–510. <https://doi.org/10.1130/G31789.1>
- Kranenburg, W. M., Geyer, W. R., Garcia, A. M. P., & Ralston, D. K. (2019). Reversed lateral circulation in a sharp estuarine bend with weak stratification. *Journal of Physical Oceanography*, 49(6), 1619–1637. <https://doi.org/10.1175/JPO-D-18-0175.1>
- Leonard, L. A. (1997). Controls of sediment transport and deposition in an incised mainland marsh basin, southeastern North Carolina. *Wetlands*, 17(2), 263–274. <https://doi.org/10.1007/BF03161414>
- Liu, Z., Fagherazzi, S., & Cui, B. (2021). Success of coastal wetlands restoration is driven by sediment availability. *Communications Earth & Environment*, 2(1), 1–9. <https://doi.org/10.1038/s43247-021-00117-7>
- Marion, C., Anthony, E. J., & Trentesaux, A. (2009). Short-term (≤ 2 yrs) estuarine mudflat and saltmarsh sedimentation: High-resolution data from ultrasonic altimetry, rod surface-elevation table, and filter traps. *Estuarine, Coastal and Shelf Science*, 83(4), 475–484. <https://doi.org/10.1016/j.ecss.2009.03.039>
- Mariotti, G., & Fagherazzi, S. (2013). Critical width of tidal flats triggers marsh collapse in the absence of sea-level rise. *Proceedings of the National Academy of Sciences*, 110(14), 5353–5356. <https://doi.org/10.1073/pnas.1219600110>
- Mariotti, G., Kearney, W. S., & Fagherazzi, S. (2016). Soil creep in salt marshes. *Geology*, 44(6), 459–462. <https://doi.org/10.1130/G37708.1>
- Martinez, J. M., Guyot, J. L., Filizola, N., & Sondag, F. (2009). Increase in suspended sediment discharge of the Amazon River assessed by monitoring network and satellite data. *Catena*, 79(3), 257–264. <https://doi.org/10.1016/j.catena.2009.05.011>
- Meade, R. H. (1969). Landward transport of bottom sediments in estuaries of the atlantic coastal plain. *Journal of Sedimentary Research*, 39(1), 222–234. <https://doi.org/10.1306/74D71C1C-2B21-11D7-8648000102C1865D>
- Milliman, J. D., & Farnsworth, K. L. (2011). *River discharge to the coastal ocean: A global synthesis*. Cambridge University Press.
- Möller, I., Kudella, M., Rupprecht, F., Spencer, T., Paul, M., van Wesenbeeck, B. K., et al. (2014). Wave attenuation over coastal salt marshes under storm surge conditions. *Nature Geoscience*, 7(10), 727–731. <https://doi.org/10.1038/ngeo2251>
- Morris, J. T., Barber, D. C., Callaway, J. C., Chambers, R., Hagen, S. C., Hopkinson, C. S., et al. (2016). Contributions of organic and inorganic matter to sediment volume and accretion in tidal wetlands at steady state. *Earth's Future*, 4(4), 110–121. <https://doi.org/10.1002/2015EF000334>
- Peteet, D. M., Nichols, J., Kenna, T., Chang, C., Browne, J., Reza, fmm, et al. (2018). Sediment starvation destroys New York City marshes' resistance to sea level rise. *Proceedings of the National Academy of Sciences*, 115(41), 10281–10286. <https://doi.org/10.1073/pnas.1715392115>
- Pethick, J. S. (1981). Long-term accretion rates on tidal salt marshes. *Journal of Sedimentary Research*, 51(2), 571–577. <https://doi.org/10.1306/212F7CDE-2B24-11D7-8648000102C1865D>
- Ralston, D. K., Yellen, B., & Woodruff, J. D. (2021). Watershed suspended sediment supply and potential impacts of dam removals for an estuary. *Estuaries and Coasts*, 44(5), 1195–1215. <https://doi.org/10.1007/s12237-020-00873-3>
- Redfield, A. C. (1972). Development of a new England salt marsh. *Ecological Monographs*, 42(2), 201–237. <https://doi.org/10.2307/1942263>
- Reed, D. J. (1989). Patterns of sediment deposition in subsiding coastal salt marshes, Terrebonne Bay, Louisiana: The role of winter storms. *Estuaries*, 12(4), 222–227. <https://doi.org/10.2307/1351901>

- Reed, D. J., Spencer, T., Murray, A. L., French, J. R., & Leonard, L. (1999). Marsh surface sediment deposition and the role of tidal creeks: Implications for created and managed coastal marshes. *Journal of Coastal Conservation*, 5(1), 81–90. <https://doi.org/10.1007/BF02802742>
- Sanks, K. M., Shaw, J. B., & Naithani, K. (2020). Field-based estimate of the sediment deficit in Coastal Louisiana. *Journal of Geophysical Research: Earth Surface*, 125(8), e2019JF005389. <https://doi.org/10.1029/2019JF005389>
- Schuerch, M., Rapaglia, J., Liebetrau, V., Vafeidis, A., & Reise, K. (2012). Salt marsh accretion and storm tide variation: An example from a barrier Island in the North sea. *Estuaries and Coasts*, 35(2), 486–500. <https://doi.org/10.1007/s12237-011-9461-z>
- Smith, J. E., Bentley, S. J., Snedden, G. A., & White, C. (2015). What role do hurricanes play in sediment delivery to subsiding river Deltas? *Scientific Reports*, 5(1), 17582. <https://doi.org/10.1038/srep17582>
- Sousa, A. I., Lillebø, A. I., Pardo, M. A., & Caçador, I. (2010). Productivity and nutrient cycling in salt marshes: Contribution to ecosystem health. *Estuarine, Coastal and Shelf Science*, 87(4), 640–646. <https://doi.org/10.1016/j.ecss.2010.03.007>
- Talke, S. A., Kemp, A. C., & Woodruff, J. (2018). Relative sea level, tides, and extreme water levels in Boston harbor from 1825 to 2018. *Journal of Geophysical Research: Oceans*, 123(6), 3895–3914. <https://doi.org/10.1029/2017JC013645>
- Temmerman, S., Govers, G., Wartel, S., & Meire, P. (2003). Spatial and temporal factors controlling short-term sedimentation in a salt and freshwater tidal marsh, Scheldt estuary, Belgium, SW Netherlands. *Earth Surface Processes and Landforms*, 28(7), 739–755. <https://doi.org/10.1002/esp.495>
- Tetra Tech EC, Inc. (2005). *Comprehensive site Assessment Report: Fireworks I*. Retrieved from <http://eeonline.eea.state.ma.us/EEA/File-Viewer/Scanned.aspx?id=206833>
- Thieler, E. R., Smith, T. L., Knisel, J. M., & Sampson, D. W. (2013). *Massachusetts shoreline change Mapping and analysis Project, 2013 update (U.S. Geological Survey open-File Report 2012–1189* (p. 42). Retrieved from <http://pubs.usgs.gov/of/2012/1189/>
- Town of Hanover, MA. (2008). *Fireworks I site*. Retrieved from https://www.hanover-ma.gov/sites/g/files/vyhli6666t/file/file/2008_fact_sheet.pdf
- Turner, R. E., Baustian, J. J., Swenson, E. M., & Spicer, J. S. (2006). Wetland sedimentation from hurricanes Katrina and Rita. *Science*, 314(5798), 449–452. <https://doi.org/10.1126/science.1129116>
- US Air Force. (2014). *Final Environmental Assessment to renovate Fourth Cliff recreational area at Hanscom Air Force Base*. Retrieved from <https://apps.dtic.mil/sti/pdfs/ADA617408.pdf>
- U.S. Fish and Wildlife Service. (2013). *National Wetlands Inventory website*. U.S. Department of the Interior, Fish and Wildlife Service. Retrieved from <http://www.fws.gov/wetlands/>
- U.S. Geological Survey. (2016). *The StreamStats program for Massachusetts*. Retrieved from <http://water.usgs.gov/osw/streamstats/massachusetts.html>
- Wang, J., Dai, Z., Mei, X., & Fagherazzi, S. (2020). Tropical cyclones significantly alleviate Mega-deltaic erosion induced by high riverine flow. *Geophysical Research Letters*, 47(19), e2020GL089065. <https://doi.org/10.1029/2020GL089065>
- Ward, L. (2004). Variations in physical properties and water quality in the Webhannet River estuary (wells National Estuarine Research Reserve, Maine). *Journal of Coastal Research*, 45, 39–58. *Special Issue*. <https://doi.org/10.2112/SI45-039.1>
- Weston, N. B. (2014). Declining sediments and rising seas: An unfortunate convergence for tidal wetlands. *Estuaries and Coasts*, 37(1), 1–23. <https://doi.org/10.1007/s12237-013-9654-8>
- Woodruff, J. D., Venti, N. L., Mabee, S. B., DiTroia, A. L., & Beach, D. (2021). Grain size and beach face slope on paraglacial beaches of New England, USA. *Marine Geology*, 438, 106527. <https://doi.org/10.1016/j.margeo.2021.106527>
- Yellen, B. C., Woodruff, J. D., Baranes, H. E., Geyer, W. R., Engelhart, S., & Griswold, F. (2022). Salt marsh response to increased tidal inundation. *Earth and Space Science Open Archive*. <https://doi.org/10.1002/essoar.10510795.1>
- Zhao, L., Chen, C., Vallino, J., Hopkinson, C., Beardsley, R. C., Lin, H., & Lerczak, J. (2010). Wetland-estuarine-shelf interactions in the Plum Island Sound and Merrimack River in the Massachusetts coast. *Journal of Geophysical Research: Oceans*, 115(C10). <https://doi.org/10.1029/2009JC006085>